Layer-by-Layer Self-Assembly of Alumosilicate−Polyelectrolyte Composites: Mechanism of Deposition, Crack Resistance, and Perspectives for Novel Membrane Materials

N. A. Kotov,*,† S. Magonov,‡ and E. Tropsha§

Department of Chemistry, Oklahoma State University, Stillwater, Oklahoma 74078, Digital Instruments, 520 E. Montecito Street, Santa Barbara, California 93103, and Becton-Dickinson, 21 Davis Drive, P.O. Box 12016, Research Triangular Park, North Carolina 27709-2016

Received September 26, 1997. Revised Manuscript Received December 17, 1997

The morphology and gas permeation properties of montmorillonite−polyelectrolyte self-assembled multilayer systems have been investigated. Without any special pretreatment, a stable film of montmorillonite−polymer composite was assembled on a hydrophobic poly(ethyleneterephthalate) support by means of layer-by-layer deposition. All individual alumosilicate platelets were found to be oriented in parallel to the substrate, while their surface density strongly depended on the nature of the polyelectrolyte (charge and molecular weight). The organic−inorganic films were found to be very flexible and crack-resistant even under a considerable mechanical stress. This opened a possibility to preclude gas diffusion through defects and to design highly selective ultrathin membranes. A permeation rate of oxygen was found to decrease 6.6 times for ca. 200 nm montmorillonite/poly(diallyldimethylammonium) chloride film, while a permeation rate of aqueous vapors did not change at all. This effect was attributed to the dominance of solution/adsorption permeation mechanism over the Knudsen diffusion. This fact made the montmorillonite−polyelectrolyte multilayers stand out among other thin films for which the diffusion through defects was found to be the primary mechanism of gas permeation. This finding demonstrated both practical and fundamental importance of hybrid thin films that combined the properties of both organic and inorganic materials.

Introduction

Layer-by-layer (LBL) self-assembly of oppositely charged polyelectrolytes[1−6] and other species such as proteins,[7−12] conducting polymers,[13,14] zirconium phosphate,[15] dyes,[16−18] metal nanoparticles,[19−23] semiconductor quantum dots,[24] alumosilicates,[25−31] and graphite oxide[32] can be considered as an alternative to the Langmuir−Blodgett deposition, chemical vapor deposi-

* Corresponding author. E-mail: kotov@okway.okstate.edu.
† Oklahoma State University.
‡ Digital Instruments.
§ Becton-Dickinson.

(1) Lvov, Y.; Essler, F.; Decher, G. *J. Phys. Chem.* **1993**, *97*, 13773.
(2) Decher, G.; Lvov, Y.; Schmidt, J. *Thin Solid Films* **1994**, *244*, 772−777.
(3) Decher, G.; Hong, J.; Schmitt, J. *Thin Solid Films* **1992**, *210/211*, 831−835.
(4) Lvov, Y.; Decher, G.; Mohwald, H. *Langmuir* **1993**, *9*, 481−486.
(5) Lvov, Y.; Decher, G. *Crystallogr. Rep.* **1994**, *39*, 628−647.
(6) Lvov, Y.; Haas, H.; Decher, G.; Mohwald, H.; Kalachev, A. *J. Phys. Chem.* **1993**, *97*, 12835−12841.
(7) Lvov, Y.; Haas, H.; Decher, G.; Mohwald, H.; Mikhailov, A.; Mtchedlishvily, B.; Morgunova, E.; Vainstein, B. *Langmuir* **1994**, *10*, 4232−4236.
(8) Lvov, Y.; Ariga, K.; Kunitake, T. *Chem. Lett.* **1994**, 2323−2326.
(9) Lvov, Y.; Ariga, K.; Ichinose, I.; Kunitake, T. *J. Am. Chem. Soc.* **1995**, *117*, 6117.
(10) Onda, M.; Lvov, Y.; Ariga, K.; Kunitake, T. *Biotechnol. Bioeng.* **1996**, 51.
(11) (a) Lvov, Y.; Ariga, K.; Ichinose, I.; Kunitake, T. *J. Chem. Soc., Chem. Commun.* **1995**, 2312. (b) Ariga, K.; Lvov, Y.; Ichinose, I.; Kunitake, T. *J. Am. Chem. Soc.* **1997**, *119*, 2224−2231.
(12) Hodak, J.; Etchenique, R.; Calvo, E.; Singhal, K.; Bartlett, P. N. *Langmuir* **1997**, *13*, 2708−2716.
(13) Cheung, J. H.; Fou, A. F.; Rubner, M. F. *Thin Solid Films* **1994**, *244*, 985−989.
(14) Ferreira, M.; Cheung, J. H.; Rubner, M. F. *Thin Solid Films* **1994**, *244*, 806−809.
(15) Keller, S. W.; Kim, H. N.; Mallouk, T. E. *J. Am. Chem. Soc.* **1994**, *116*, 8817−8818.
(16) Zhang, X.; Gao, M.; Kong, X.; Sun, Y.; Shen, J. *J. Chem. Soc., Chem. Commun.* **1994**, 1055.
(17) Cooper, T. M.; Campbell, A. L.; Crane, R. L. *Langmuir* **1995**, *11*, 2713.
(18) Ichinoze, I.; Fujiyoshi, K.; Mizuki, S.; Lvov, Y.; Kunitake, T. *Chem. Lett.* **1996**, 257.
(19) Keller, S. W.; Kim,; H. N.; Mallouk, T. E. *J. Am. Chem. Soc.* **1994**, *116*, 8817−8818.
(20) Feldheim, D. L.; Crabar, K. C.; Natan, M. J.; Mallouk, T. E. *J. Am. Chem. Soc.* **1996**, *118*, 7640−7641.
(21) Schmitt, J.; Decher, G.; Dressik, W. J.; Branduo, S. L.; Geer, R. E.; Shashidhal, R.; Calvert, J. *Adv. Mater.* **1997**, *9*, 61−65.
(22) Freeman, R. G.; Grabar, K. C.; Allison, K. J.; Bright, R. M.; Davis, J. A.; Guthrie, A. P.; Hommer, M. B.; Jackson, M. A.; Smith, P. C.; Walter, D. G.; Natan, M. J. *Science* **1995**, *267*, 1629−1632.
(23) Grabar, K. C.; Freeman, R. G.; Hommer, M. B.; Natan, M. J. *Anal. Chem.* **1995**, *67*, 735−743.
(24) Kotov, N. A.; Dékány, I.; Fendler, J. H. *J. Phys. Chem.* **1995**, *99*, 13065−13069.
(25) Kleinfeld, E. R.; Ferguson, G. S. *Chem. Mater.* **1995**, *7*, 2327−2331.
(26) Kleinfeld, E. R.; Ferguson, G. S. *Chem. Mater.* **1996**, *8*, 1575−1578.
(27) Kleinfeld, E. R.; Ferguson, G. S. *Science* **1994**, *265*, 370−373.
(28) Kleinfeld, E. R.; Ferguson, G. S. *Mater. Res. Soc. Symp. Proc.* **1995**, *369*, 697−702.

S0897-4756(97)00649-2 CCC: $15.00
Published on Web 02/18/1998

tion, spin-coating, and other methods of preparation of advanced thin films. Among other benefits, this technique permitted preparation of hybrid organic−inorganic composites that possessed a unique set of properties typical for both constituents. Multilayer assemblies produced by this method were shown to be perspective candidates for a number of high-tech applications.[33−40] In particular, recent studies have demonstrated a considerable potential of hybrid LBL assemblies for advanced optical and electronic coatings.[41−49]

The most substantial advantages of the LBL self-assembly are (1) ultimate simplicity of the deposition procedure and (2) quite accurately controlled *average* thicknesses of polyelectrolyte layers. If compared to Langmuir−Blodgett multilayers (LB), the films produced by alternate adsorption on polyelectrolytes were shown to be substantially less ordered. The interlayer roughness was comparable or even exceeded the thickness of an individual layer both for polyelectrolyte−polyelectrolyte,[50] nanoparticle−polyelectrolyte,[21,24] and alumosilicate−polyelectrolyte superlattices.[31] The washed out boundaries between the layers limited the applicability of such multilayer systems for the preparation of sophisticated layered nanostructures with possible applications in electronics. Regardless of this constraint, the idea of layered coatings of composite materials remained very attractive and was expected to be quite productive for the preparation of functional films in which the combination of properties of both inorganic and organic materials could be utilized. The control over an average film thickness with a precision approaching 1 nm augmented the value of such multilayer assemblies.

In organic−inorganic composite films, relatively high interlayer roughness could become a friend rather than a foe in the case of gas separation membranes where mechanical stability, as well as diffusion, solubility, adsorption, and other integral characteristics, is more influential than continuity of an individual layer. Four different mechanisms for separation of gases through a porous membrane can be identified: (a) gas enrichment based on the differences in molecular weights of the components due to a different velocity of gas molecules in pores (Knudsen diffusion), (b) molecular sieving due to differences in molecular diameter, (c) selective dissolution or selective adsorption due to a difference in chemical properties, (d) partial condensation of some components in pores with exclusion of others. The first two mechanisms allowed efficient separation of gases only with inordinately large differences in molecular weights, whereas the last two afforded selectivity in gases based on differences in chemical properties with the masses of the molecules nearly identical.

Extreme thinness and the molecularly ordered structure of the LB films induced broad interest to their barrier properties. Presumably, chemical interactions with the two-dimensional crystal lattice of surfactants were expected to promote very specific gas separation while small thicknesses could provide high permeation rates. A number of different LB systems were investigated on gas permeability properties. They were first reported for classical LB amphiphilies such as stearic and oleic acids[51] for which a substantial reduction of the gas flux was observed. Later, it was confirmed that, indeed, well-packed crystalline films represented a substantial obstacle for gas diffusion; however, mostly defects (cracks) in the films, rather than chemical interactions with the matrix, were responsible for gas permeation.[52] Unfortunately, this type of gas penetration did not support good selectivity because the gases to be separated normally had rather little difference in molecular masses ($Mw(O_2) = 32$ and $Mw(N_2) = 28$) which determined the diffusion rate in this case.

Therefore, polymeric or polymerizable monolayers have been used with the anticipation that they were mechanically stronger and more flexible.[53−60] Consequently, the appearance of cracks could have been minimized or eliminated completely. Nonetheless, even in two-dimensional polymer networks of amphiphilic

(29) Lvov, Y.; Ariga, K.; Ichinose, I.; Kunitake, T. *Langmuir* **1996**, *12*, 3038−3044.
(30) Kotov, N. A.; Dékány, I.; Fendler, J. H. *J. Phys. Chem.* **1995**, *99*, 13065−13069.
(31) Kotov, N. A.; Haraszti, T.; Turi, L.; Zavala, G.; Geer, R. E.; Dékány, I.; Fendler, J. H. *J. Am. Chem. Soc.***1997**, *119* (29), 6821−6832.
(32) Kotov, N. A.; Dékány, I.; Fendler, J. H. *Adv. Mater.* **1996**, *8*, 637−641.
(33) Giannelis, E. P. *Adv. Mater.* **1996**, *8*, 29−35.
(34) Ruiz-Hitzky, E.; Aranda, P.; Casal, B.; Galvan, J. C. *Adv. Mater.* **1995**, *7*, 180−184.
(35) Moya, J. *Adv. Mater.* **1995**, *7*, 185−189.
(36) Chen, Z.; Samuelson, L. A.; Akkara, J.; Kaplan, D. L.; Gao, H.; Kumar, J.; Marx, K. A.; Tripathy, S. K. *Chem. Mater.* **1995**, *7*, 1779−1783.
(37) Wang, L.; Schindler, J.; Thomas, J. A.; Kannewurtf, C. R.; Kanatzidis, M. G. *Chem. Mater.* **1995**, *7*, 1753−1755.
(38) Reference deleted in proof.
(39) Deng, Q.; Moor, R. B.; Mauritz, K. A. *Chem. Mater.* **1995**, *7*, 2259−2268.
(40) Bortun, A.; Strelko, V. V.; Jaimez, E.; Garcia, J. R.; Rodriguez, J. *Chem. Mater.* **1995**, *7*, 249−251.
(41) Lvov, Y.; Yamada, S.; Kunitake, T. *Thin Solid Films* **1997**, *300*, 107−112.
(42) Wischerhoff, E.; Laschewsky, A.; Mayer, B. *Proceedings of European Conference on Organized Films*, ECOF 6, Sheffield, U.K., 11−14 Sept 1996, 3.15.
(43) Laschewsky, A.; Mayer, B.; Wischerhoff, E.; Arys, X.; Bertrand, P.; Delcorte, A.; Jonas, A. *Thin Solid Films* **1996**, *284−285*, 334−337.
(44) Saremi, F.; Maasen, E.; Tieke, B.; Jordan, G.; Rammensee, W. *Langmuir* **1995**, *11*, 1068−1071.
(45) Cooper, T. M.; Campbell, A. L.; Crane, R. L. *Abstr. Pap. Am. Chem. Soc.* **1995**, *209* (APR), 60.
(46) Keller, S. W.; Saupe, G. B.; Mallouk, T. E. *Abstr. Pap. Am. Chem. Soc.* **1995**, *209* (APR), 540.
(47) Gregoriu, V. G.; Hapanowicz, R.; Clark, S. L.; Hammond, P. T. *Appl. Spectrosc.* **1997**, *51* (4), 470−476.
(48) Baur, J.; Rubner, M.; Reynolds, J. R.; Kim, S.; Arnold, F.; Dang, T. *Abstracts of 1996 Fall Meeting of the Materials Research Society*, Boston, MA, December 2−6, 1996; p 135.
(49) Saremi, F.; Lang, G.; Tieke, B. *Adv. Mater.* **1996**, *8*, 923−926.
(50) Losche, M.; Schmitt, J.; Bouwman, W. G.; Kjaer, K.; Decher, G. *Abstr. European Conference on Organized Films ECOF 6*; Sheffield, U.K., Sept 11−14, 1996; p O38. Decher, G.; et al. *Thin Solid Films* **1992**, *210−211*, 831. Schmitt, J.; Decher, G.; et al. *Macromolecules* **1993**, *26*, 7058. Decher, G.; Lvov, Y.; Schmitt, J. *Thin Solid Films* **1994**, *244*, 772.
(51) Rose, G. D.; Quinn, J. A. *Science* **1968**, *159*, 636−637.
(52) Gains, G. L., Jr.; Ward, W. J., III. *Coll. Interfacial. Sci.* **1977**, *60*, 207.
(53) Bruinsma, P. J.; Sturesson, C.; Spooner, G. J. R.; Cooleman, L. B.; Stroeve, P. *Polym. Prepr.* **1991**, *32*, 242−243.
(54) Bruinsma, P. J.; Spooner, G. J. R.; Cooleman, L. B.; Koren, R.; Sturesson, C.; Stroeve, P. *Thin Solid Films* **1992**, *210/211*, 440−442.
(55) Higashi, N.; Kunitake, T.; Kajiyama, T. *Polym. J.* **1987**, *19*, 289−291.
(56) Miyashita, T.; Konno, M.; Matsuda, M.; Saito, S. *Macromolecules* **1990**, *23*, 3531−3533.
(57) Lee, B.-J.; Kunitake, T. *Langmuir* **1992**, *8*, 2223.
(58) Lee, B.-J.; Kunitake, T. *Langmuir* **1994**, *10*, 557−562.
(59) Lefevre, D.; Porteu, F.; Balag, P.; Roulliay, M.; Zalczer, G.; Palacin, S. *Langmuir* **1993**, *9*, 150−161.
(60) Bruinsma, P. J.; Stroeve, P. *Thin Solid Films* **1994**, *242*, 151−156.

molecules, cracks and pinholes were found to play the major role in gas permeation,[61−63] which, at least in part, was likely to be due to high glass transition temperature of the polymers employed. Again, the Knudsen diffusion was shown to dominate over the solubility mechanism at room temperature. On the positive side, the role of chemical properties and the role of selective gas adsorption augmented above 60 °C when the mobility of polymer chains increased; the maximum in CO_2/N_2 selectivity was achieved at 72 °C and was equal to 4.5.

Very recently, the first data on the application of layer-by-layer self-assembly of polyelectrolytes for the preparation of gas separation membranes have been reported.[64] P. Stroeve and co-workers applied a multilayer assembly of poly(allylamine) and poly(styrenesulfonate) onto a hydrophobic microporous poly(propylene) membrane Celgard 2400 and on a hydrophobic solid dimethyl silicone membrane. Gas permeation measurements through the Celgard membrane revealed the dominance of diffusion through cracks. On the contrary, for dimethyl silicon supports, high CO_2/N_2 selectivities of up to 10.4 at 20 °C were observed. Unfortunately, at 50 °C the selectivity factor decreased down to 8.3, again due to crack formation as was evidenced by optical microscopy.

Therefore, the defects in the thin film prepared by both LB and layer-by-layer self-assembly must be considered as the primary problem for the producing of advanced gas separation membranes. In this study we approached this problem from the position that the method of sequential adsorption was quite perspective for the membrane design because it offered very good control over the total thickness, reasonable control over the internal structure, and eventually, the ease of industrial realization. Therefore, we focused on the materials aspect of this problem in order to identify proper combination of alternating layers. Organic−inorganic hybrid assemblies were quite obvious candidates for the further studies for they were reported to possess high tensile strength and high-temperature resistance of ceramics, as well as structural versatility of organic materials.[65−71]

In this publication, the study on structure, gas permeation properties, and initial steps of deposition of thin films of alumosilicate−polyelectrolyte composites prepared by layer-by-layer deposition is presented. Experimental results indicated that this system had a potential to significantly improve existing ultrathin membranes because of the substantially reduced tendency to crack on bendable substrates. This property originated in the multilayer structure of the films which can be represented as a sequence of alternating thin layers of alumosilicate sheets and polyelectrolytes. Laterally oriented montmorillonite particles provided excellent gas barrier properties while the polyelectrolyte layers served as an interlayer binder and effective adhesion agent to solid substrates. Virtual absence of deep cracks enabled the adsorption mechanism of gas permeation to prevail over the Knudsen diffusion through defects. As a result, the role of gas penetration via dissolution and/or absorption mechanisms is believed to increase as compared to that of previously tested multilayer assemblies.

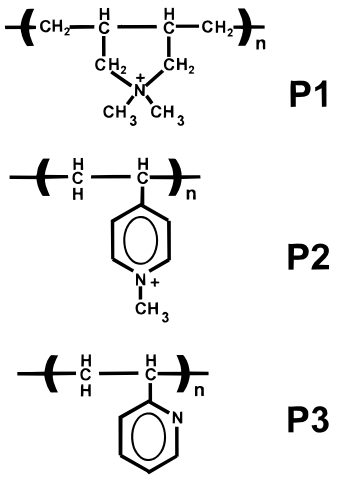

Figure 1. Structure of the polyelectrolytes used for preparation of montmorillonite−polyelectrolyte LBL assemblies.

Experimental Section

Materials. Poly(diallyldimethylammonium) chloride, P1, Mw = 400 000−500 000 (Aldrich, high molecular weight); (poly(4-vinyl-1-methylpyridinium) bromide, P2, M_w = 50 000 (Polysciences, Inc.); and poly(2-vinylpyridine), P3, M_w = 200 000−400 000 (Polysciences, Inc.) were used as received (Figure 1). Stock solutions of P1 and P2 were prepared by dissolving an appropriate amount of the commercial 20% solution in deionized water (18 MΩ/cm). The stock solution of P3 was made by dissolving a weighted amount of the polymer in water at pH = 1.5 (soluble only at low pH).

A ready-to-use sample of sodium montmorillonite, M, was a generous gift from the laboratory of Prof. I. Dékány, Attila József University, Szeged, Hungary. It was prepared by suspending in water 10 g/L of the original clay mineral from Mad, Hungary. The suspension was allowed to settle for 17 h. The supernatant was removed and converted into a sodium form by stirring with 1.0 N NaCl. The sodium montmorillonite particles were then separated by centrifugation, washed, and dialyzed to remove the excess electrolyte. Analysis: SiO_2 = 61.58%, Al_2O_3 = 22.15%, Fe_2O_3 = 4.5%, CaO = 0.14%, Na_2O = 3.18%, alkaline earth metals = 0.95%, water hydration = 8.0%; specific surface area (determined by N_2 adsorption at 77 K, using the BET equations) = 58 m^2/g. Basal distance in

(61) Albert, O.; Laschewsky, A.; Ringsdorf, H. *J. Membr. Sci.* **1985**, *22*, 187−197.
(62) Corner, M.; Janout, V.; Regen, S. L. *J. Am. Chem. Soc.* **1993**, *115*, 1178−1180.
(63) Bruinsma, P. J.; Strove, P.; Hoffmann, C. L.; Rabolt, J. F. *Thin Solid Films* **1996**, *284−285*, 713−717.
(64) Stroeve, P.; Vasques, V.; Coelho, M. A. N.; Rabolt, J. F. *Thin Solid Film* **1996**, *284−285*, 708−712.
(65) Messersmith, P. B.; Giannelis, E. P. *Chem. Mater.* **1994**, *6*, 1719.
(66) Giannelis, E. P.; Mehrotra, V.; Tse, O.; Vaia, R. A.; Sung, T.-C. In *Synthesis and Processing of Ceramics: Scientific Issues*; Rhine, W. E., Shaw, T. M., Gottshall, R. J., Chen, Y., Eds.; MRS Proc.: Pittsburg, PA, 1992.
(67) Vaia, R. A.; Vasudevan, S.; Krawiec, W.; Scanlon, L. G.; Giannelis, E. P. *Adv. Mater.* **1995**, *7*, 154.
(68) Kojima, Y.; Usuki, A.; Kawasumi, M.; Okada, A.; Fukushima, Y.; Kuraichi, T.; Kamigaito, O. *J. Mater. Res.* **1993**, *8*, 1185.
(69) Yano, K.; Usuki, A.; Okada, A.; Kuraichi, T.; Kamigaito, O. *J. Polym. Sci.: Part A: Polym. Chem.* **1993**, *31*, 2493.
(70) Wang, M. S.; Pinnavia, T. J. *Chem. Mater.* **1994**, *6*, 468.
(71) Lan, T.; Pinnavia, T. J. *Chem. Mater.* **1994**, *6*, 2216. Pinnavaia, T. J. *Science* **1983**, *220*, 365−369.
(72) Mizutani, Y.; Nakamura, S.; Kaneko, S.; Okamura, K. *Ind. Eng. Chem. Res.* **1993**, *32*, 221−227.
(73) van Olphem, H. *An Introduction to Clay Colloid Chemistry*; Wiley: New York, 1977.
(74) Norris, K. *Discuss. Faraday Soc.* **1954**, *18*, 120.

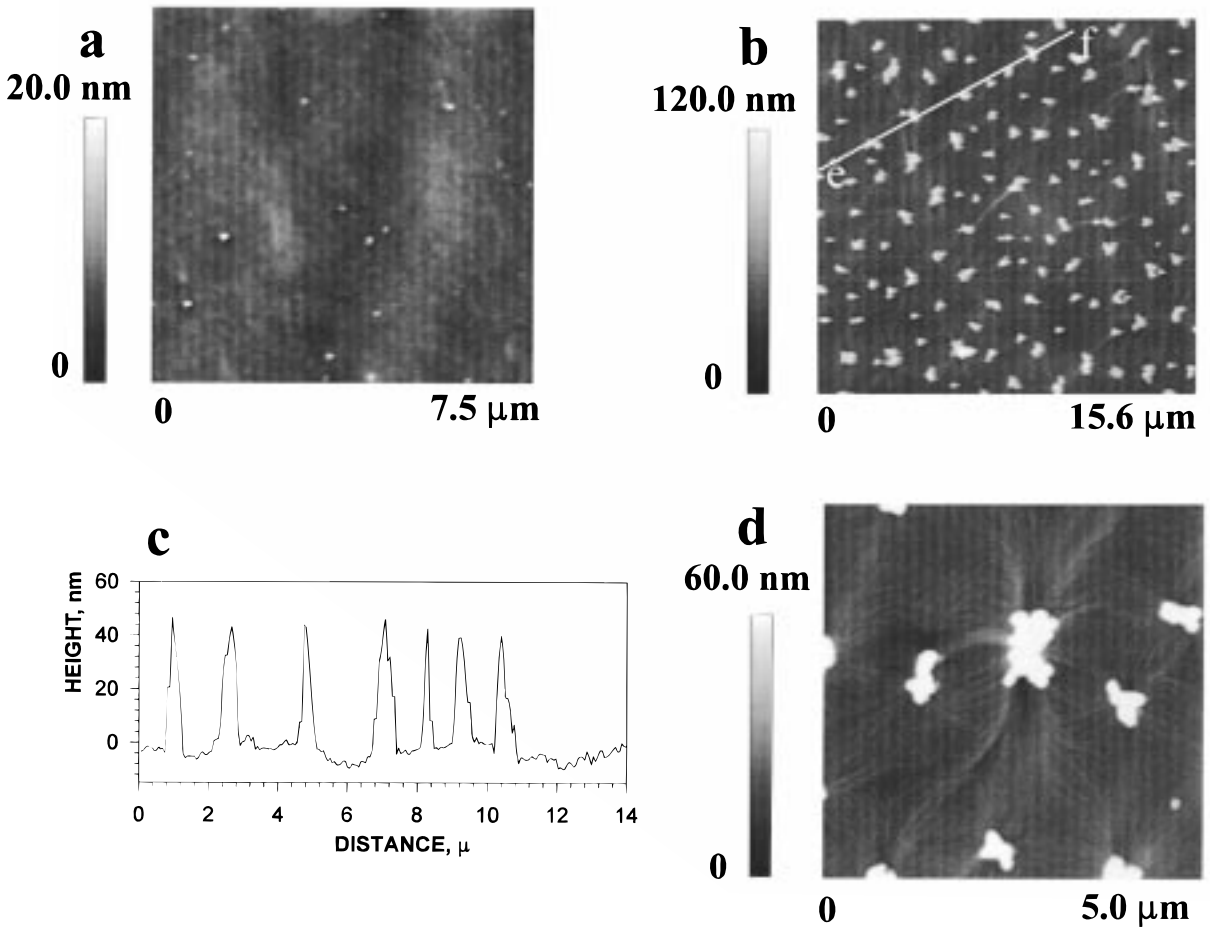

Figure 2. Atomic force microscopy image of (a) untreated PET substrates, (b, d) the PET substrate after immersion into P1 solution followed by thorough rinsing with deionized water and drying, and (c) the cross section along the e−f line on image b.

air-dried Na-montmorillonite was identical to literature values[73−76] and was equal to 1.25 nm.

Montmorillonite dispersion for the self-assembly of clay−polyelectrolyte multilayers was prepared by sonicating 1.5 g of purified, air-dried, sodium montmorillonite in 500 mL of distilled water for 20 min. A rougher fraction was sedimented, and the supernatant was sonicated again for 20 min. After two centrifugations at 3000 rpm, the top fraction was separated, poured into a shallow plastic container that was used as an immersion bath for gas permeation substrates.

Silica wafers for atomic force microscopy were purchased from Virginia Semiconductor Co. Their average roughness did not exceed 5 Å, and they were used as received.

Samples for O_2 and H_2O permeability measurements were made on poly(ethyleneterephthalate) films (PET) obtained from DuPont Chemicals (Mylar D) with a characteristic density of 1.39 g/cm^3 and a glass transition temperature of 120 °C. The thickness of the films was 25 μm.

Preparation of the Films. Clay/polyelectrolyte multilayers were deposited on poly(ethyleneterephthalate) 14.5 × 14.5 cm^2 sheets without any pretreatment of the PET surface. Overall, the process of the self-assembly consisted of the cyclic repetition of four steps: (1) immersion of the substrate into an aqueous 0.1% (w/v) solution of a polymer for 1−2 min, (2) rinsing with ultrapure water for 30 s in three different containers, (3) immersion into an aqueous dispersion of montmorillonite for 1 min, and (4) final rinsing with deionized water for 30 s in two different containers. The buildup of the film always started with the exposure of the substrate to a solution of a corresponding positively charged polyelectrolyte for 5 min.

The following notations will be used throughout the paper: n = number of deposition cycles (i.e., the number of repetitions of steps 1−4); the film formed as a result of n deposition cycles will be referred to as $(P/M)_n$.

The kinetics of the montmorillonite adsorption was found to be quite rapid. After 30 s and after 16 h of exposure to the montmorillonite dispersion the density of platelets was found to be identical (not shown).

Gas Permeation Measurements. Permeance measurements for oxygen were obtained by using temperature-controlled OxTran 2/20 equipment from Modern Controls, Inc. The oxygen gradient across the film system was kept at 1 atm 100% oxygen concentration on the upstream side of the film vs 1 atm 98% nitrogen/2% hydrogen carrier gas on the downstream side. Oxygen permeating through the sample film was entrained in a nitrogen carrier gas stream on the opposite side of the film and detected by a Coulometric sensor. Water vapor content on both sides of the test film was kept at 0% relative humidity. The data were taken at a constant temperature of 30 °C. Permeability units used to report the permeation rate of oxygen were cm^3/m^2 day atm and corresponded to the amount of oxygen in cm^3 that passed through a PET membrane with a thickness of 25 μm (see above) of an area of one m^2 per day when a gradient of oxygen pressure between both sides of a membrane was equal to 1 atm. For uncoated PET it was 80 ± 0.5 cm^3/m^2 day atm.

Water permeance measurements were obtained by using Permatran W600 equipment from Modern Controls, Inc.

(75) Lagaly, G.; Weiss, A. *Angew. Chem.* **1971**, *83*, 580.
(76) Dékány, I.; Szántó, F.; Weiss, A.; Lagaly, G. *Ber. Bensen−Ges. Phys. Chem.* **1985**, *89*, 62−67.
(77) Oosawa, F. *Polyelectrolytes* Marcel Decher, Inc.: New York, 1971.
(78) Rice, S. A.; Nagaswa, M.; Morawetz, H. *Polyelectrolytes Solutions. A Theoretical Introduction., An International Series of Monographs and Textbooks*; Kaplan, N. O., Sheraga, H. A., Eds.; Academic Press: London, 1961.

Relative humidity on the upstream side of the film was kept at 100% vs 0% on the downstream side for all experiments. Water vapor permeating through the sample film was introduced into an IR sensor by nitrogen carrier gas. An electrical signal was produced in proportion to the amount of water vapor permeating through the sample. Steady-state transmission data were taken at 30 °C. Permeability units used to report the permeation rate of water were different than those for oxygen, namely cm^3/m^2 day. They corresponded to the volume of aqueous vapor in cm^3 that passed through a membrane with a thickness of 25 μm of an area of one m^2 per day when a gradient of relative humidity across the membrane was 100%. For uncoated PET, the permeability rate was 30 $\pm$ 0.5 cm^3/m^2 day.

Films were mounted on either instrument and conditioned for a minimum of 24 h at a temperature of interest before the measurements were taken.

AFM Images. Atomic force microscopic (AFM), measurements were performed, in air, by using a Nanoscope IIIa system (Digital Instruments Inc., Santa Barbara, CA) operating in the tapping mode. The samples of PET substrate and silicon wafers were mounted on metal disks with adhesive surface. TESP silicon tips (wafer 10555 L087) with a cantilever length of 125 μm and a characteristic frequency of 300−330 kHz were employed for image acquisition. The autotune function of the Nanoscope software was used to find the resonance frequency of a noncontact probe. No change in the frequency was observed for a particular probe even after several days of work. The scanning head was mounted on a tripod with a concrete vibration isolation pad suspended on rubber cables (Digital Instruments Inc.).

SEM Microscopy was performed by using an Amray 1645 instrument equipped with a LaB_6 electron source and operated at 10 kV.

Results and Discussion

Polyelectrolytes were known to adsorb strongly to oppositely charged surfaces. For polycationite−polyanionite multilayers researchers normally pretreated the substrate surface by physical or chemical means so that ionizable groups could be generated.[1−6] The analysis of free energy of electrostatic interaction between polyelectrolytes demonstrated that hydrophobic interactions had to provide a considerable part of the total free energy in the layer-by-layer self-assembly. Therefore, we were interested whether it was possible to successfully deposit a $(P/M)_n$ layer onto an uncharged hydrophobic surface such as PET. Initial stages of the LBL deposition were studied by AFM, which greatly assisted in gaining a better understanding of the mechanism of multilayer buildup on hydrophobic surfaces. After initial exposure of PET to the solution of P1, small "islands" (500−900 nm in diameter and 50 nm heigh) of the polyelectrolyte were found on the surface (Figure 2a,b,c). Interestingly enough, the strands of polyelectrolyte formed a curious matrix of parallel lines gravitating toward nearest polyelectrolyte microdroplet (Figure 2d), which originated, probably, in the flow pattern when the hydrophilic layer of aqueous solution collapsed on the hydrophobic surface. Importantly, the AFM image of PET bearing P1 did not change at all after additional thorough rinsing in ample amount of water and drying in the stream of nitrogen. It demonstrated that the hydrophobic interactions played an important role in adhesion of P1 to PET. Electrostatic attraction to occasionally formed charged surface defects (for example, −COOH groups from oxidized polymer backbone) would certainly promote formation of the adsorption layer; however, this process was likely to be of minor importance since the density of ionizable groups of the surface of hydrophobic PET was supposed to be quite low.

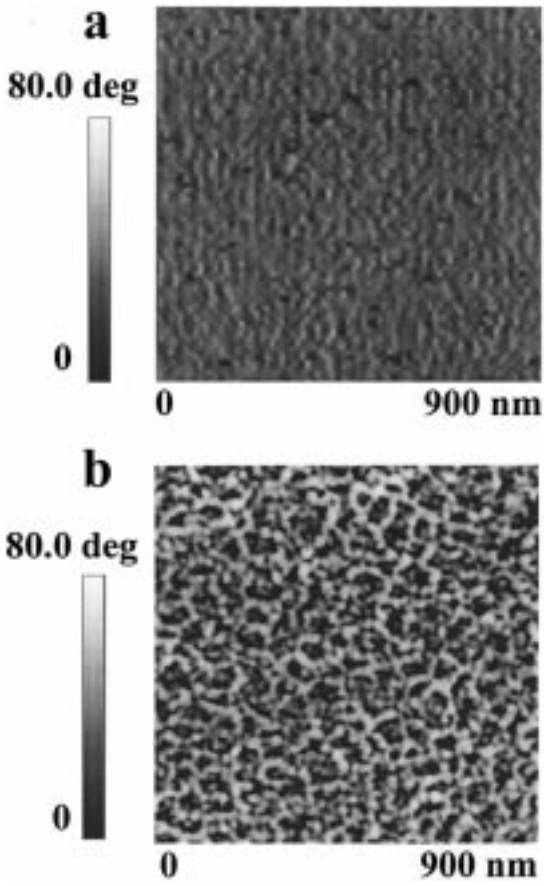

Figure 3. Phase modulation image of (a) untreated PET substrates and (b) the ET substrate after immersion into P1 solution followed by thorough rinsing with deionized water and drying. The image was taken in the area between elevated microdroplets of polyelectrolyte.

Between elevated polyelectrolyte microdroplets, the surface was covered with a uniform layer of chainlike formations that could be particularly well-resolved in the phase image mode of AFM (Figure 3). Although it is quite possible that this AFM image represented the network of single polyelectrolyte molecules enlarged in the $X-Y$ plane by the tip effect, at the present moment it is difficult to assign the observed objects to any sort of molecular aggregates until they are studied on atomically flat surfaces. At any rate, the difference between the uncoated PET surface and the PET−P1 surface was quite prominent leaving no doubts about the adsorption of P1 on PET.

Immersion in montmorillonite dispersion did not initially result in a noticeable change of the surface topography (not shown). Individual clay platelets were initially difficult to visualize due to intrinsic roughness of the underlying surface. After the third deposition cycle one could easily observe adsorbed alumosilicate species on the strands of the polyelectrolyte (Figure 4). Their size was close to the expected diameter of the platelets (100−200 nm). In small quantities, large platelets (ca. 500 nm) were observed as well. After the fourth deposition cycle the PET surface became hydro-

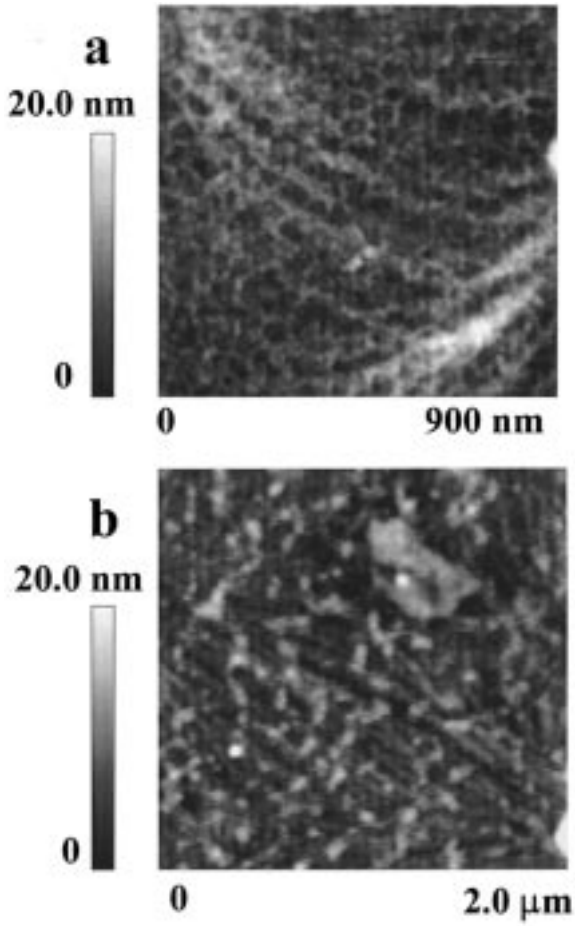

Figure 4. Atomic force microscopy image of (a) the PET substrate after immersion into P1 solution followed by thorough rinsing with deionized water and drying and (b) the PET substrate after three deposition cycles.

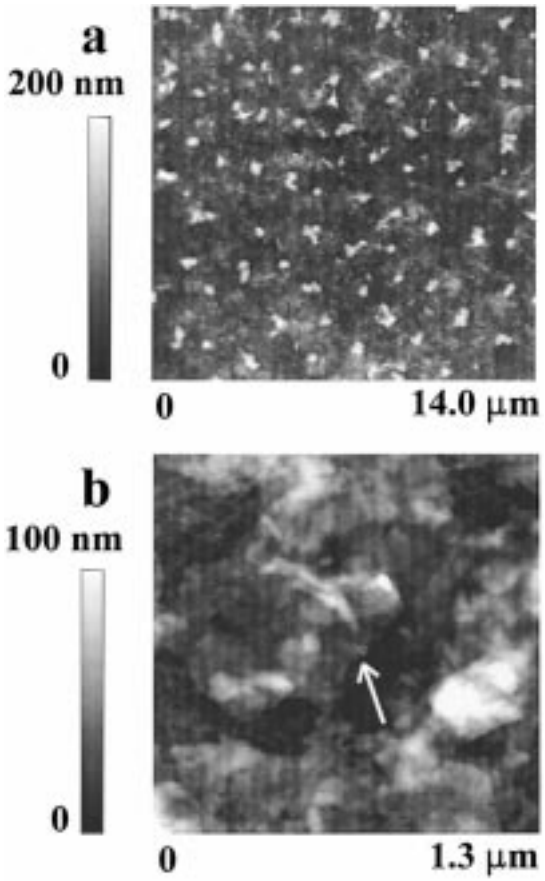

Figure 5. Atomic force microscopy image of the $(P1/M)_{30}$ film on the PET substrate. The arrow on image b shows the individual clay platelet on the surface of $(P1/M)_{30}$.

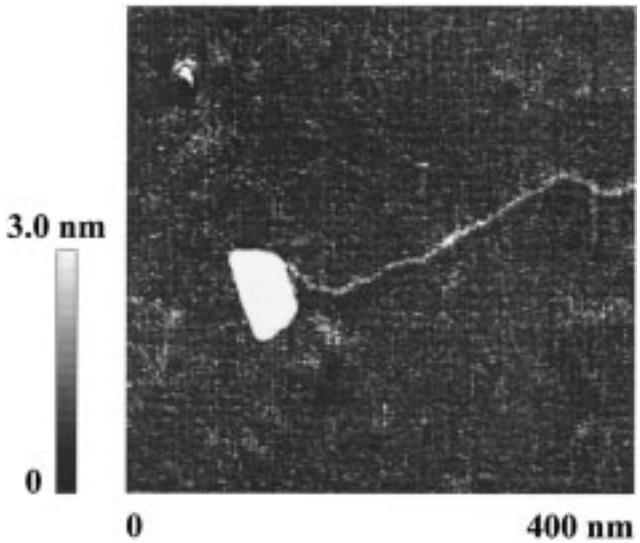

Figure 6. Atomic force microscopy image of an alumosilicate platelet adsorbed to P3. The sample, i.e., the $(P3/M)_1$ film, was prepared on a silicon wafer as described in the Experimental Section. The diameter of the polyelectrolyte chain appears to be larger than expected due to the tip effect.

philic and remained so for the rest of the deposition process.

The surface structure in advanced stages of LBL ($n > 4$) was investigated for $(P1/M)_{30}$ (Figure 5). It was uniformly covered by alumosilicate platelets. One could notice that bright high spots (Figure 5a) had the distribution pattern and dimensions similar to the previously seen microdroplets of polyelectrolyte (Figure 2b). Since their height was comparable to the total thickness of $(P1/M)_{30}$ (50 nm vs 120 nm (see ref 31)) and the thickness of the film was quite uniform, initially elevated spots maintained their elevated position and distribution even after 30 deposition cycles.

The effect of gradual hydrophilization of the surface is a characteristic feature of $(P1/M)_n$. It was associated with a large aspect ratio of alumosilicate sheets. Being on average 100 nm in diameter, a montmorillonite platelet was able to cover a much larger area than the polyelectrolyte chain it was adsorbed to (Figure 6). In general, both for PET and other hydrophobic surfaces, the newly formed negatively charged surface of alumosilicate formed patches of a much friendlier surface for the second adsorption cycle of positively charged polyelectrolyte. In turn, it resulted in greater quantities of the polymer adsorbed to the substrate. The following layer of alumosilicate further expanded the area of the film. This process continued until rapidly growing "islands" of highly hydrophilic $(P/M)_n$ layers merged together. Quite rough but continuous composite films were obtained on hydrophobic silicon wafers[26] and even on Teflon.[30]

Due to the layer-by-layer character of the deposition, atomic force microscopy permitted the assessment of the internal structure of the $(P/M)_n$ multilayers. The structural property that singled out $(P/M)_n$ multilayers from

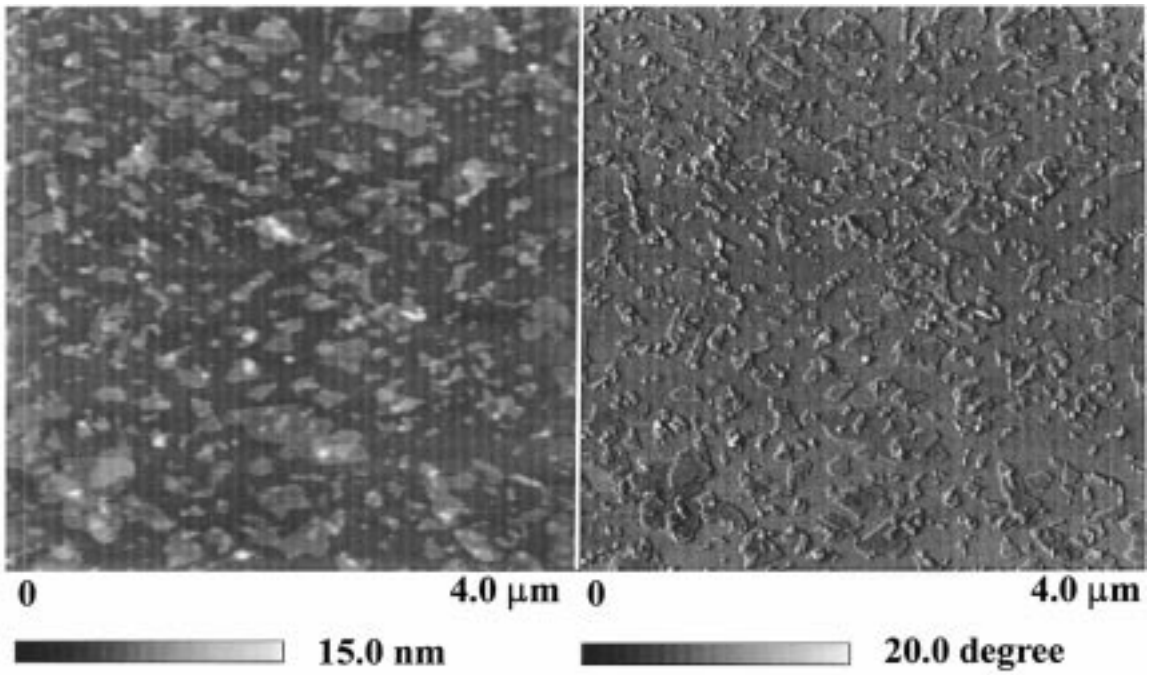

Figure 7. Atomic force microscopy images in topography (a) and phase modulation (b) modes of a silicon wafer with $(P1/M)_1$ film. Substrate exposure to the filtered (0.22 μm) montmorillonite dispersion was reduced to 8 s in order to obtain images of well-separated platelets.

other clay−polymer composites, actively studied nowadays, was the parallel to the substrate orientation of montmorillonite platelets. The consistent alignment of alumosilicate sheets could be seen for small and large numbers of $(P/M)_n$ layers deposited on PET and silicon wafers (Figures 5b and 7). It was a result of a tendency of the adsorbate to minimize both the electrostatic and nonelectrostatic component of the energy of the system. Such ordering was a specific structural property of $(P/M)_n$ films imparted by the deposition technique. To the best of our knowledge, the like composites were impossible to obtain by any other means, except, probably, by using a sophisticated alternating layer LB trough[79] with alternate deposition of monolayer of hydrophobic clays and polymers.

The surface density of platelets was found to be markedly different for various polyelectrolytes (Figure 8). For P1, montmorillonite formed a virtually continuous layer of platelets (Figure 8a). At a higher magnification, one could see sparingly distributed shallow depressions in the otherwise quite uniform film. They appeared when irregular alumosilicate sheets or their short stacks of 2−4 montmorillonite units produced a gap between adjacent particles comparable to their diameter. Subsequently, these depressions were most likely to be filled with polyelectrolyte and capped by a new montmorillonite layer via a self-healing mechanism observed for etched pits on silicon.[31]

For P2, the overall density of platelets noticeably decreased (Figure 8b), and for P3 only very few small particles were shown to adsorb (Figure 8c). The low adsorptivity of montmorillonite on P3, as compared to P1 and P2, was associated with virtually negligible ionization of poly(2-vinylpyridine) at neutral pH (pH = 6.2). In the case of P2, the diminished propensity of M to adsorb on it was likely to be the consequence of a lower molecular weight as compared to P1 (50 000 vs 500 000 au). The effect of charge reversal and the ability to bridge the gaps between particles were directly related to the molecular weight of the polymer. The similar dependence of the surface density of M was observed for P1 of lower molecular masses.[80]

A very important feature of these films can be seen in Figure 9. As was already noted, quite often alumosilicate platelets formed face-to-face agglomerates, and occasionally, the top particle happened to be larger than the bottom one. Interestingly, instead of protruding into the space above it, the top sheet wrapped around the edge of the bottom sheet. This behavior resembled that of a fabric rather than of a rigid solid substance intuitively expected from alumosilicates. This demonstrated that montmorillonite, when separated into single sheets, was, in fact, a very soft and flexible material.

The flexibility and a rather large area covered by a single particle jointly contributed to the unique resilience of alumosilicate−polyelectrolyte multilayers to the physical breakdown. LB films from surfactants, polymers, and LBL assemblies of oppositely charged polyelectrolytes were prone to the proliferation of microcracks when subjected to external pressure. Consequently, their performance as ultrathin membranes suffered. A $(P1/M)_{30}$ film deposited on PET did not reveal the formation of a significant number of cracks after being intensively bent, warped, and subjected to fast oscillating deformations caused by the stream of nitrogen directed laterally at the edge of the substrate ("flag-in-the-wind").[81] In fact, we checked ten 15 μm windows in various places of the surface and found small cracks only in two of them (Figure 10), which was

(79) Kotov, N. A.; Meldrum, F. C.; Fendler, J. H.; Tombacz, E.; Dekany, I. *Langmuir* **1994**, *10*, 3797.

(80) Kotov, N.; Magonov, S. Unpublished results.

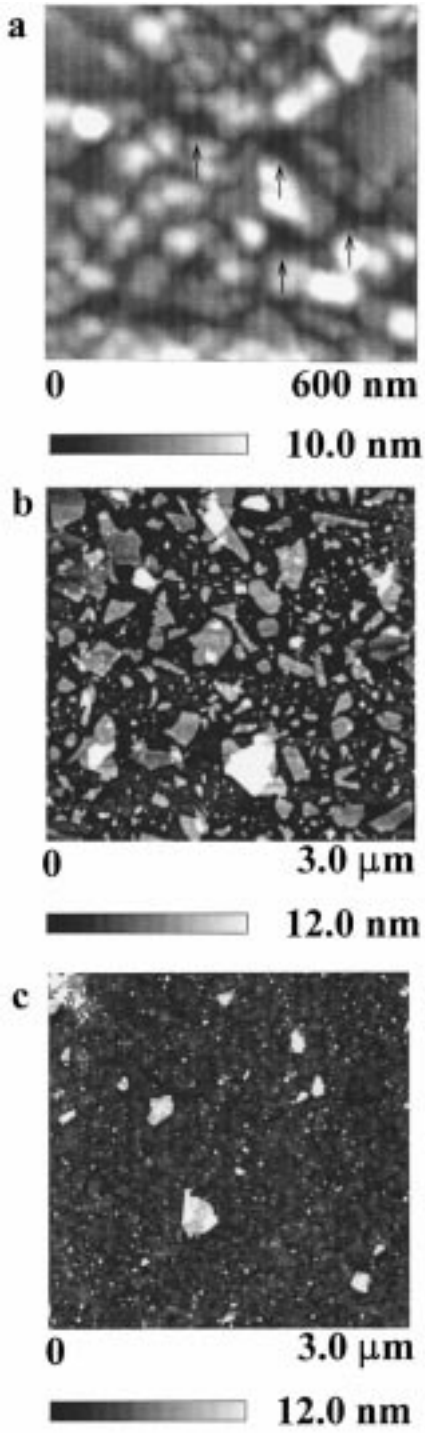

Figure 8. Atomic force microscopy image of (a) $(P1/M)_1$, (b) $(P2/M)_2$, and (c) $(P3/M)_1$ on a silicon wafer. Arrows in image a denote the gaps between individual platelets or their aggregates.

markedly different as compared to the microscopy images published previously.[64] The profile of the cracks (Figure 10c) suggested that they did not penetrate deep into the bulk of the film but rather disrupted only the top few $(P/M)_n$ layers ($n \approx 10$). Note that the thickness of the entire $(P1/M)_{30}$ film could be estimated on the basis of the previously determined average thickness

(81) Note that the physical stress normally experienced by a gas separation membrane is supposed to be smaller than that because they are usually prepared as a thin layer topping a rigid microporous substrate (porous glass).

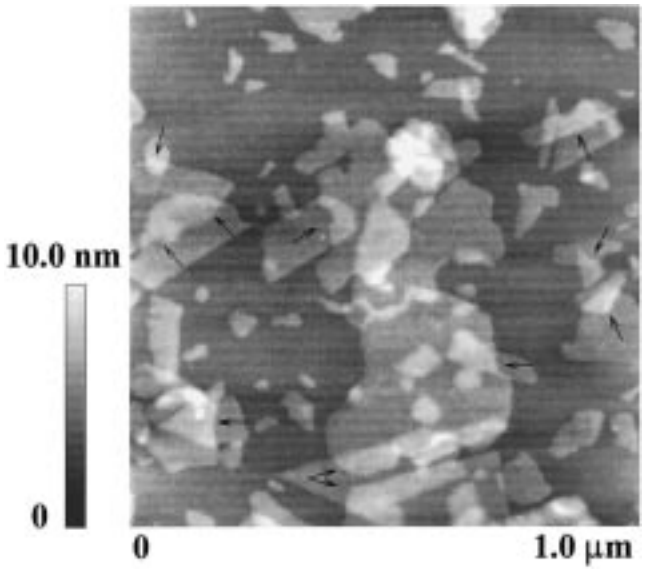

Figure 9. Atomic force microscopy image of $(P1/M)_1$ film on silicon wafer. Exposure to the filtered (0.22 μm) montmorillonite dispersion was reduced to 15 s. Arrows indicate overlapping montmorillonite platelets. Top platelets conform to the topography of the bottom particle and the underlying substrate, which indicates that they are not rigid but rather soft and flexible.

of a single (P/M) stratum, i.e., 4 nm[82] which yielded the total thickness of $d = 30 \times 4 = 120$ nm.

Observation of narrow gaps and deep wells with high aspect ratio by AFM can be limited by physical dimensions of pyramidal AFM tip. We considered that the verification of the quite remarkable properties of montmorillonite−polyelectrolyte films by an independent method would be desirable. The absence of cracks after the mechanical stress was confirmed by scanning electron microscopy image (Figure 11). The features observed on this image are virtually identical to that of AFM scans.

Overall flexibility and planar orientation of the platelets were excellent starting points for the design of a new type of gas separation membranes. For $(P/M)_n$ layers, gas permeation properties of oxygen and aqueous vapor were investigated by varying n, the type of the polymer, and the permeating gas (Figures 12and 13). The permeation rate of O_2 linearly decreased with n for all $(P/M)_n$ systems studied (Figure 12). Although the number of layers and the total thickness of the film was relatively small, $d = 200$ nm for $(P1/M)_{50}$, a marked decrease in the permeability of oxygen for $(P1/M)_n$ and $(P2/M)_n$ films was observed. The permeation rate for $(P1/M)_{50}$ decreased by 6.6 times as compared to that for the uncoated PET film (Figure 12). This result was particularly meaningful taking into account that the

(82) In ref 31 we found that the thickness of a P/M film deposited in one cycle is 3.9 ± 0.5 nm. This value is in a good agreement with that obtained from the Kiessig fringes in the X-ray diffraction measurements, 4 ± 0.5 nm. In similar systems a one-cycle thickness increment was reported to be 3.6 ± 0.4,[27] and 3.2−3.8 nm.[29] The observed small variations are likely to be connected with a particular experimental method (surface plasmon spectroscopy,[31] X-ray,[29] or elipsometry[27]) used for thickness determination as well as with a particular clay sample (montmorillomite[29,31] and hectorite[27]). The size of clay platelets (100−150,[31] 40,[27] and 500 nm[29]) and surface charge may also contribute to the difference in vertical packing due to partial overlap of the platelets and electrostatic repulsion between them.

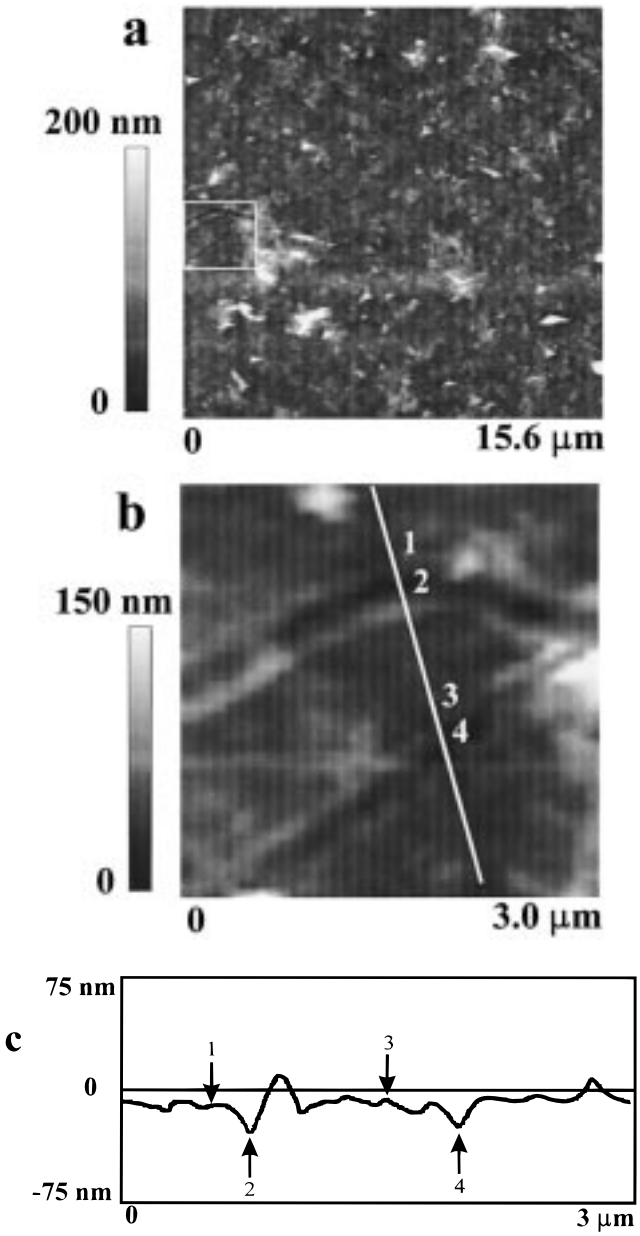

Figure 10. AFM results for $(P1/M)_{30}$ film on PET substrate subjected to mechanical stress: (a) image one out of two 15.6 × 15.6 μm^2 scans where cracks in the film were observed (total 10 scans, in other images no cracks could be seen); (b) enlarged area highlighted by a white rectangle on image a; (c) cross section along the white line on image b.

overall thickness, $d_{(P/M)} + d_{PET}$, of the membrane increased only by 0.8%.

For P2 multilayer assemblies, the rate of oxygen permeation decreased to a smaller extent than the rate for the same number of layers of P1 (Figure 12): for $(P2/M)_{50}$ the permeability rate has dropped by 2 times. For the three different polyelectrolytes studied, i.e., poly(diallyldimethylammonium) chloride (P1), (poly(4-vinyl-1-methylpyridinium) bromide (P2), and poly(2-vinylpyridine) (P3), the variation of the barrier function of prepared multilayer assemblies can be related to the average density of clay particles observed in AFM (Figure 5−7): the greater the percentage of the area covered by alumosilicate, the greater the inhibition of the oxygen flux. The retention of oxygen for $(P/M)_{10}$ films decreased in the order P1 > P2 > P3 (Table 1).

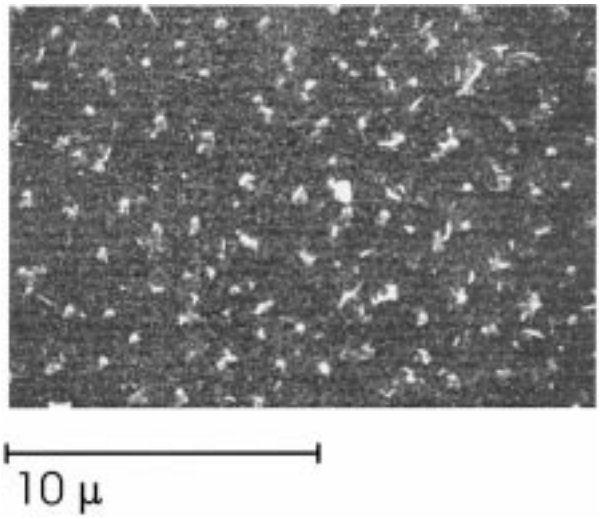

Figure 11. Scanning electron microscopy image of $(P1/M)_{30}$ film on PET substrate subjected to mechanical stress.

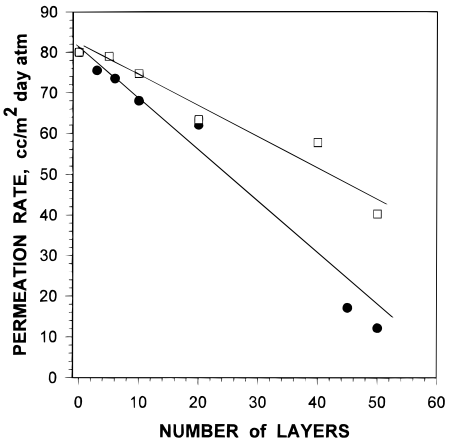

Figure 12. Dependence of the permeation rate of oxygen through PET substrate coated with $(P1/M)_n$ (●) and $(P2/M)_n$ (□) film on the number of deposition cycles *n*.

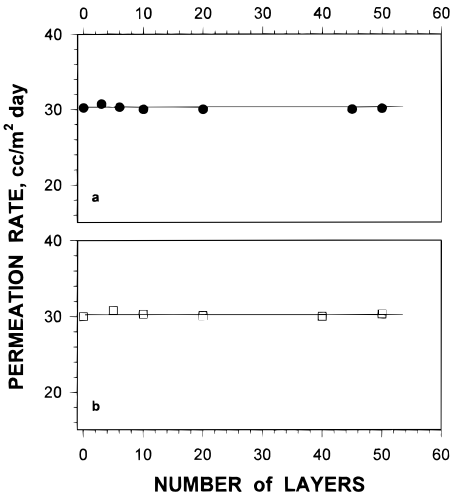

Figure 13. Dependence of the permeation rate of aqueous vapor through PET substrate coated with (a) $(P1/M)_n$ and (b) $(P2/M)_n$ film on the number of deposition cycles *n*.

Most interestingly, the $(P/M)_n$ coating selectively retained oxygen while not affecting the flux of water molecules through the film. The permeation rate for water vapors did not change at all regardless of the number of layers for all films studied (Figure 13). We

Table 1. Permeation Rates of Oxygen for $(P/M)_{10}$ Assemblies Based on Various Polyelectrolytes

polyelectrolyte used for self-assembly	no. of deposition cycles	permeation rate of oxygen cm^3/m^2 day atm
P1	10	68.0
P2	10	74.7
P3	10	75.3

have not observed even a slight reduction of water permeation even for a quite thick polymer−montmorillonite film prepared in 50 deposition cycles. This fact could not be explained from the position of a simple diffusion of water molecules through pores or defects because the total diffusion path was increased and the barrier function of laterally oriented alumosilicate sheets was considerable (see above). We believe that being fairly hydrophilic in nature, $(P/M)_n$ composites selectively adsorbed/dissolved water vapors while the penetration of nonpolar oxygen molecules was obstructed by montmorillonite. The realization of a similar separation principle was attempted for other ultrathin films.[53−63] However, extensive cracking of the coatings did not permit proper detection of the effect. For $(P/M)_n$ multilayers, the diffusion through the defects was at least strongly diminished, if not eliminated, due to inordinary flexibility of the film. Unlike most other thin film gas membranes, dissolution and/or adsorption mechanisms dominated over the Knudsen diffusion in $(P/M)_n$ multilayers. This demonstrated a considerable potential of organic−inorganic thin film composites for the membrane design as well as fundamental advantages of hybrid materials.

The selection of water vapor and oxygen for permeability measurements was dictated by applications in the medical industry. The difference in polarity between the two gases is quite large, and therefore, the two gases can be considered as a convenient model system for studying thin film membranes based on the difference in chemical properties. The performance of LBL composite film for separation of nonpolar gases such as O_2 and N_2 is planned to be the subject of an upcoming publication.

Conclusion

Montmorillonite−polyelectrolyte LBL films were shown to self-assemble on flexible PET substrates. AFM imags demonstrated that the individual alumosilicate sheets are unexpectedly flexible and oriented in parallel to the substrate. Layered montmorillonite−polyelectrolyte composite film exhibited exceptionally high mechanical strength and resilience to crack proliferation. This makes this layer a quite promising material for the preparation of gas separation and other membranes. The relative permeativity of oxygen and water through coated $(P/M)_n$−PET was rationalized as the result of gas diffusion by the solubility/adsorption mechanism as opposed to Knudsen diffusion through defects typical for thin film gas separation membranes.

Acknowledgment. N.A.K. thanks Oklahoma State University Research Foundation for the financial support of this research. Special thanks go to Dr. S. Whang from the Center of Laser and Photonics Research for his generous help with scanning electron microscopy.

CM970649B